



Mixed oxides supported low-nickel formulations for the direct amination of aliphatic alcohols with ammonia



A. Tomer^{a,b}, Z. Yan^b, A. Ponchel^{a,*}, M. Pera-Titus^{b,*}

^a Univ. Artois, CNRS, Centrale Lille, ENSCL, Univ. Lille, UMR 8181, Unité de Catalyse et de Chimie du Solide (UCCS), F-62300 Lens, France

^b Eco-Efficient Products and Processes Laboratory (E2P2L), UMI 3464 CNRS – Solvay, 3966 Jin Du Road, Xin Zhuang Ind. Zone, 201108 Shanghai, China

ARTICLE INFO

Article history:

Received 14 June 2017

Revised 27 July 2017

Accepted 15 August 2017

Keywords:

n-Octanol

Ammonia

Direct amination

CeO₂-Al₂O₃

Nickel

ABSTRACT

The present study focuses on the selective synthesis of primary amines from aliphatic alcohols and ammonia using alumina-ceria supported nickel formulations based on very low nickel loading (≤ 2 wt%) and without any additive or external H₂ supply. The effect of the catalyst preparation methods and modes of nickel impregnation were studied in detail and comprehensively characterized. The best formulation afforded 80% *n*-octanol conversion with 78% selectivity to *n*-octylamine at optimized reaction conditions, which were far better than control catalysts and benchmark Ni-alumina formulations relying on high Ni loadings. The enhanced activities of the alumina-ceria supported nickel catalysts was attributed to three combined effects: (1) a higher reducibility of surface nickel oxide species, (2) the genesis of very small and homogeneously distributed nickel nanoparticles (2–3 nm), and (3) a strong decline in the formation of nickel aluminates. Furthermore, unlike benchmark Ni catalysts, these formulations afforded a higher resistance to leaching.

© 2017 Elsevier Inc. All rights reserved.

1. Introduction

Synthetic amines are extensively used as intermediates for the production of pharmaceuticals, agrochemicals, detergents, polymers, varnishes and dyes [1,2]. Alkylamines constitute a particular family of amines derived from fatty acids, olefins or alcohols issued either from natural sources (fats, oils) or from petrochemical raw materials. The global fatty amines market was valued at US\$ 1.7 Mn in 2014 and is estimated to grow to US\$ 2.2 Mn by 2020 mainly driven by the Asia-Pacific region excluding Japan (APEJ), accounting for more than 25% of the revenue share in 2014 [3]. The world market of alkylamines is segmented in 6 sectors: (1) water treatment, (2) agrochemistry, (3) oilfield, (4) asphalt additives, (5) anti-caking, and (6) others (personal care, mining, fabric softening, paints and coatings) [4,5]. Water treatment constitutes the largest market with more than 29% of the global revenue (2014), and it is anticipated to grow by 4.7% until 2020 [3].

Various methods are available for synthesizing alkylamines, including alkyl halide amination, reductive amination of ketones or aldehydes, hydroamination of olefins, hydroaminomethylation, and nitrile hydrogenation [6–11]. However, most of these methods suffer from poor selectivity to the desired amines, use toxic or

hazardous reagents, consume H₂ stoichiometrically, and/or produce significant amount of waste (e.g., salts). As an alternative, the alkylation of amines with (bio)alcohols appears as an eco-efficient method for amine production as water is generated as the main byproduct [12].

The most extended catalysts for the direct synthesis of amines from alcohols rely on homogeneous Ru and Ir complexes operating via the borrowing H₂ or H₂ auto-transfer mechanism without external H₂ supply [13–18]. In parallel, heterogeneous catalysts based on Raney Ni [19,20], and Ni [21–25], Cu [26–29], NiCu [30–32], NiCuFeO_x [33] and NiCuZn [34] nanoparticles supported over alkaline or amphoteric oxides have shown high versatility for the additive-free alkylation of amines and ammonia with aromatic and aliphatic alcohols. In particular, Shimizu and co-workers recently showed that 10 wt%Ni/θ-Al₂O₃ could afford high yields (70–96%) in the reaction of primary and secondary alcohols with excess ammonia at 160 °C for 13–72 h [23]. The major shortcoming of non-noble based catalysts is often ascribed to the use of large metal contents (most often >15 wt%), as well as to their heterogeneous particle size distributions and low metal dispersion, which impacts their activity for amination. High-Ni loaded formulations may result in the formation of a NiO crystalline phase on the support, resulting into large Ni particles and accordingly low Ni dispersion during the reduction process. Furthermore, high-Ni loaded catalysts are prone to Ni leaching upon exposure to

* Corresponding authors.

E-mail addresses: anne.ponchel@univ-artois.fr (A. Ponchel), marc.pera-titus-ext@solvay.com (M. Pera-Titus).

ammonia and polar solvents, thereby affecting not only the catalytic activity, but also favoring the contamination of the amine product by Ni. In this context, the development of eco-efficient processes with stable and selective heterogeneous catalysts minimizing the Ni content for the direct amination of alcohols is hour of need.

Ceria is a well-known promoter that can modify the structural or electronic properties of catalysts in many industrial reactions such as automotive exhaust gas conversion (i.e. 3-way catalysts) [35–37], methane reforming with CO₂ and/or with steam, and water-gas shift reactions [38–42]. In particular, ceria is well known to enhance the thermal stability of alumina [43,44], reduce the Ni particle size and mitigate coke formation and metal sintering in Ni/ γ -Al₂O₃ catalysts, especially for CO methanation and steam-reforming reactions [39,40,42,45,46]. In parallel, several patents have reported the amination of aliphatic and ethoxylated alcohols relying mostly on Ni, Cu or Co, either in bulk form or supported over single and mixed oxides containing rare-earth oxides [47–52]. In particular, a process patented by Imperial Chemical Industries (UK) describes the amination of ethanol in the presence of a catalyst comprising NiO-CoO-Al₂O₃-CeO₂ prepared by co-precipitation in the presence of sodium carbonate [48]. The catalyst afforded 98% ethanol conversion to ethylamine, diethylamine and triethylamine with 43%, 44% and 13% yields, respectively, with the simultaneous formation of high boiling byproducts. A patent by BASF SE disclosed the use of a catalyst based on Cu supported over La₂O₃-Al₂O₃ support for the liquid-phase synthesis of secondary amines from primary and secondary alcohols such as ethanol, isopropanol and cyclohexanol and primary amines [52].

To the best of our knowledge, no report is available in neither the open nor the patent literature on low-Ni formulations (≤ 2 wt % Ni) for the direct amination of alcohols, especially over alumina. This is probably due to the fact that low-Ni formulations are poorly active for amination due to the formation of inactive surface Ni aluminates even when subjected to low calcination temperatures [53,54]. Ni-aluminates are also favored at higher Ni loadings (2–5 wt% Ni) at a calcination temperature >550 °C by promoting solid-state diffusion of Ni²⁺ cations into the alumina lattice [55–58]. Here we report for the first time a cooperative effect between alumina and ceria in 2 wt.%Ni/CeO₂-Al₂O₃ catalysts affording high activity and selectivity to primary amines in the liquid-phase direct amination reaction of *n*-octanol with ammonia.

2. Experimental

2.1. Materials

γ -Al₂O₃ (Puralox Sasol Scca-5/170, 154 m²/g), CeO₂ (Solvay HSA5, 250 m²/g), were used as supports for catalyst synthesis. Cerium nitrate hexahydrate (Ce(NO₃)₂·6H₂O, >99 wt%) and nickel nitrate hexahydrate (Ni(NO₃)₂·6H₂O, >99 wt%), both supplied by Sigma-Aldrich, were used as precursors for the synthesis of mixed oxides and for Ni impregnation, respectively. NaOH (>98 wt%) and citric acid monohydrate (>99 wt%) were procured from J&K. Aniline, benzyl alcohol, *n*-octanol and ammonia, all supplied by J&K (99.5% purity), were used in the catalytic tests. *o*-xylene (J&K, purity 99.5%) was used as solvent in the *n*-octanol/ammonia amination tests. *N*-benzylideneaniline, *N*-benzylaniline, *N,N*-dibenzylaniline, benzonitrile, toluene, benzene, *n*-octylamine, di-*n*-octylamine, trioctylamine and octanenitrile standards for GC calibration were all purchased from J&K (purity 99.5%). All the reactants were used as received without further purification.

2.2. Catalyst synthesis

The preparation of Ni-supported mixed oxides was divided into two steps. The first step focused on the synthesis of cerium-

aluminum mixed oxides (Ce-Al) (used as supports) using two different methods, whereas the second step encompassed Ni impregnation (2 wt%) over the mixed oxides either in the dried or calcined forms.

2.2.1. Ce-Al mixed oxides prepared by wet impregnation (WI)

In a typical preparation, 5 g of γ -Al₂O₃ suspended in 70 mL of deionized water in a two-neck round bottom flask were thermally treated at 145 °C for 1 h. Subsequently, 20 mL of an aqueous solution of cerium nitrate (2.65 g) were added for 20 min at a constant stirring speed of 600 rpm using a dropping funnel. The mixture was aged for 2 h, cooled down to room temperature and the excess water was slowly removed at 60 °C using a rotary evaporator. The final solid (yellowish) was dried in an oven overnight at 120 °C and further calcined at 500 °C for 6 h using a heating rate of 3 °C min⁻¹ in a muffle furnace under static air. The solid prepared by wet impregnation is hereinafter denoted as Ce-Al_WI.

2.2.2. Ce-Al mixed oxides by the co-precipitation (PPT)

A series of Ce-Al oxides were also synthesized by a co-precipitation method as described elsewhere [59]. In a typical preparation, 5 g of γ -Al₂O₃ suspended in 50 mL of deionized water in a two-neck round bottom flask were thermally treated at 80 °C for 1 h. A 20-mL solution of cerium nitrate was added to the above solution and stirred for 5 min. Subsequently, a 25-mL solution of NaOH and citric acid (NaOH/citric acid molar ratio = 1) was added during 20 min using a dropping funnel and the solution was further aged for 2.5 h. Finally, the solid mixture was cooled down to room temperature, vacuum filtered and thoroughly washed until neutral pH using ca. 2 L deionized water. The as-obtained solid (yellowish) was dried overnight at 120 °C and further calcined at 500 °C for 6 h in a muffle furnace using a heating rate of 3 °C min⁻¹ under static air. The solid prepared by co-precipitation is hereinafter denoted as Ce-Al_PPT.

2.2.3. Ni impregnation over mixed oxides by the IWI method

Nickel (2 wt% nominal loading) was impregnated by Incipient Wetness Impregnation (IWI) over the prepared mixed oxides (Ce-Al_WI and Ce-Al_PPT). Before impregnating the nickel nitrate solution, the dried mixed oxides were divided into two halves. On the one hand, one half of the dried mixed oxide was directly impregnated with the nickel nitrate solution and then calcined at 500 °C for 6 h in a muffle furnace. On the other hand, the second half of the dried mixed oxide was subjected to a first calcination step at 500 °C for 6 h before impregnation and then calcined at similar conditions. Two routes for Ni impregnation were considered, namely after (A) and before (B) calcination. The final samples displayed different characteristic colors regardless of the support (Fig. S1).

Along with the above-mentioned catalysts, control monometallic catalysts were also prepared, namely 2Ni/Al₂O₃, 8Ni/Al₂O₃ and 2Ni/CeO₂-HS_300 (CeO₂_HS pre-calcined at 300 °C before Ni impregnation). All the catalysts were prepared by the IWI method using the nickel nitrate solution and then calcined at 400 °C for 2 h in a muffle furnace.

2.3. Catalyst characterization

The bulk metal composition of the calcined catalysts was measured using a Varian Inductively Coupled Plasma-Optical Emission Spectrometry (ICP-OES) available at the REALCAT platform at UCCS Lille. Before the analyses, the dried and ground sample (10 mg) was dissolved in 1.5 mL of concentrated *aqua regia* and 250 μ L of HF solution. The solutions were heated to 50 °C and stirred for 24 h.

The specific surface area and pore volume of the different catalysts was measured from N₂ adsorption/desorption isotherms at

–196 °C using a Micromeritics ASAP 2010 Surface Area Analyzer. The surface areas were calculated by the Brunauer-Emmett-Teller (BET) method in the relative pressure range $0.05 < P/P_0 < 0.25$, while the pore volumes were measured at $P/P_0 = 0.99$. The Barrer-Joyner-Halenda (BJH) method was used for measuring the interparticle pore size distributions. Prior to the measurements, the catalysts were degassed overnight at 100 °C.

The phases present in the different catalysts were analyzed by powder X-ray diffraction (PXRD). The PXRD patterns were recorded on a Bruker D8 Advance diffractometer in Bragg-Brentano geometry equipped with a copper anode ($\lambda = 1.5418 \text{ \AA}$) and a 1D PSD Lynxeye detector. The spectra were collected in the 2θ range 8–80° with a step size of 0.02°. The patterns were indexed using the Joint Committee on Powder Diffraction (JCPDS) database and interpreted using MDI JADE 5.0 software. The Scherrer equation was used to estimate the average size of the oxide particles from the XRD line broadening.

The Diffuse Reflectance UV-Vis (DRUV-Vis) spectra of the calcined catalysts were recorded in diffuse reflectance mode on a Lambda 650 Perkin-Elmer spectrophotometer equipped with 60 mm integrating sphere. BaSO₄ was used as standard. The Schuster-Kubelka-Munk (SKM) absorption function, expressed by $F(R) = (1 - R_\infty)^2 / 2R_\infty = K/S$, was applied for data interpretation, where R_∞ is the reflectance of a thick solid layer, and K and S indicate the absorption and diffusion coefficients, respectively.

The temperature-programmed reduction (H₂-TPR) profiles were measured on a Micromeritics AutoChem 2920 instrument equipped with a thermal conductivity detector (TCD) and a cold trap before the detector. The H₂-TPR profiles were recorded by reducing the catalysts (55 mg) under 10% H₂-Ar flow (40 mL(STP) min⁻¹) in the temperature range 30–1000 °C using a heating rate of 10 °C min⁻¹.

The CO-TPD measurements were carried out using a Micromeritics AutoChem 2920 instrument. Briefly, a known quantity of calcined catalyst (200 mg) was reduced under a H₂ flow (40 mL(STP) min⁻¹) at 580 °C for 30 min using a heating rate of 10 °C min⁻¹ and cooled down to 40 °C. Subsequently, a 3% CO-He flow (40 mL(STP) min⁻¹) was passed through the sample for 20 min. After this period, the CO excess was removed from the sample under a He flow (40 mL(STP) min⁻¹) and the CO-TPD profile was measured by monitoring the CO desorption from 40 °C to 600 °C under He using a TCD detector. The CO uptake allowed the measurement of the metal dispersion (%D), the metal surface area per gram of catalyst and per gram of metal (A_m), and the average particle size of metal (S_m).

The thermogravimetric analyses (TGA) were conducted using a TA Instruments SDT 2960 apparatus equipped with a flow gas system. The catalyst was treated from room temperature to 800 °C using a heating rate of 5 °C min⁻¹ under a 20% O₂/He mixture with

a flow rate of 75 mL(STP) min⁻¹. Approximately, 10 mg of sample was heated in an open Pt crucible.

The morphology and local composition of the different catalysts was characterized first by SEM/EDS on a Zeiss EVO-18 microscope. Subsequently, the catalysts were inspected by STEM/EDS using a 200 kV Tecnai F20 microscope equipped with a FEG electron gun, a STEM unit and an EDAX Optima T60 SDD-EDS spectrometer. The images were analyzed using EDAX Team microanalysis software. Before analysis, the solid powder was directly dispersed over the holey carbon Cu 400 mesh grid (Agar, Ref S147-4).

The surface composition of the different catalysts was analyzed by X-ray photoelectron spectroscopy (XPS) using a Kratos Axis Ultra DLD apparatus equipped with a hemispherical analyzer and a delay line detector. The spectra were recorded using an Al monochromated X-ray source (10 kV, 15 mA) with a pass energy of 40 eV (0.1 eV/step) for high resolution spectra, and a pass energy of 160 eV (1 eV/step) for survey spectrum in hybrid mode and slot lens mode, respectively. The C1 s binding energy (285.0 eV) was used as an internal reference. Prior to the measurements, the samples were reduced in a pre-treatment chamber at 580 °C for 30 min under a 10% H₂ flow (50 mL(STP) min⁻¹). Despite the intrinsic complexity of estimating the reduction level of ceria from the different components of the XPS Ce 3d core-level spectrum [60], we used the following commonly accepted expression [61]

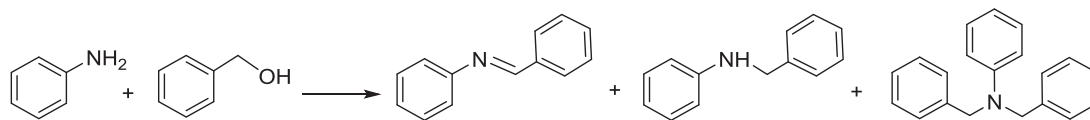
$$\text{Ce}^{3+} (\%) = \frac{v' + u'}{\sum(v + u)} \quad (1)$$

where v and u are the spin-orbit components of the $3p_{5/2}$ and $3p_{3/2}$ states of the Ce 3d core level.

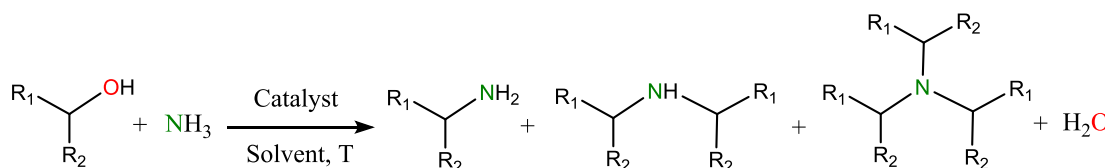
2.4. Catalytic activity measurements

The catalytic activity of the different Ni catalysts was assessed first in the model amination reaction of benzyl alcohol with aniline (Scheme 1). The reaction was performed using 2 mmol of aniline, 6 mmol of benzyl alcohol and 65 mg of pre-reduced catalyst in Biotage microwave vials under atmospheric Ar at 160 °C for 3 h and stirring speed of 600 rpm. In a second reaction, the amination of *n*-octanol with ammonia was conducted in a 30-mL stainless steel autoclave equipped with a pressure gauge and a safety valve (Scheme 2). In a given experiment, the reactor was charged with *n*-octanol (1.3 mmol) and 65 mg of pre-reduced catalyst. The reactor was sealed and evacuated by applying vacuum followed by charging ammonia (7 bar). The reactor was then placed on a hot plate equipped with a magnetic stirrer for different reaction time and temperatures.

The reactants (aniline, benzyl alcohol and *n*-octanol) and the expected products for both reactions, i.e. N-benzylideneaniline (BZIA), N-benzylaniline (BZA), N,N-dibenzylaniline (DBZA),



Scheme 1. Potential amination products in the reaction between benzyl alcohol with aniline.



Scheme 2. Potential amination products in the reaction between *n*-octanol with ammonia.

n-octylamine (OA), di-*n*-octylamine (DOA), trioctylamine (TOA), octanenitrile (ON) and *n*-octanol were analyzed and quantified using an Agilent 7890 GC equipped with a HP-5 capillary column with 5 wt% phenyl groups using biphenyl as internal standard. Mass balances were accurate to within 5% for all the catalytic tests.

The conversion of the limiting reactant (LR: aniline and *n*-octanol) and the selectivity and yield to the N-containing products were defined as follows:

$$\text{Conversion (\%)} = 1 - \frac{n_{\text{LR}}}{n_{\text{LR}}^0} \quad (2)$$

$$\text{Selectivity}_i (\%) = \frac{n_i}{n_{\text{LR}}^0 - n_{\text{LR}}} \quad (3)$$

$$\text{Yield}_i (\%) = \frac{n_i}{n_{\text{LR}}^0} \quad (4)$$

$$\text{Carbon balance} = \frac{\text{Moles of formed products} + \text{reactants}}{\text{Moles of reactants}} \quad (5)$$

where n_{LR}^0 and n_{LR} refer to the initial and final mole number of the limiting reactant, respectively, whereas n_i corresponds to the mole number of N-containing products formed. In addition to the above stated main products, toluene was formed as side product by dehydroxylation of benzyl alcohol.

Finally, the turnover number (TON) at a given time was computed by dividing the number of moles of OA formed by the number of moles of surface Ni

$$\text{TON} \left(\frac{\text{mmol OA}}{\text{mmol Ni}_{\text{surf}}} \right) = \frac{n_{\text{OA}}}{n_{\text{Ni}_{\text{surf}}}} \quad (6)$$

3. Results and discussion

3.1. Characterization

3.1.1. Textural properties

Table 1 (entries 6–10) lists the textural properties of the different calcined Ni/Ce-Al catalysts prepared in this study, whereas Figs. S2 and S3 plot the corresponding N₂ adsorption/desorption isotherms at –196 °C and pore size distributions. All the catalysts exhibit Type IV isotherms with a H2-type hysteresis loop according to the IUPAC classification that are reminiscent of mesoporous materials with a porous network consisting of interparticle pores with an ill-defined shape and a wide pore size distribution [62]. The pore size distribution of the different catalysts is affected to a certain extent by the preparation method. The catalysts synthesized by wet impregnation, i.e. Ce-Al_WI (Fig. S3, profile a), result

in more uniform and narrower pore size distributions, whereas the catalysts synthesized by the precipitation method, i.e. Ce-Al_PPT (Fig. S3, profile d), display broader distributions and slightly higher surface areas and pore volumes. Ce-Al_WI shows a lower specific surface, pore volume and mean pore size compared to the parent γ -Al₂O₃ and CeO₂-HS_300 (Table 1, entries 1, 3 and 5), suggesting a partial pore blockage by ceria particles grown over γ -alumina. Opposing this observation, Ce-Al_PPT shows comparable textural properties as in the case of γ -alumina, which can be explained by a higher dispersion of ceria.

The Ni impregnation method (i.e. before or after calcination) also impacts the textural properties of the final catalysts. A slight reduction of the specific surface area is observed for 2Ni/Ce-Al_WI(A) compared to the parent support (127 m²/g vs. 134 m²/g), whereas it keeps almost unchanged for 2Ni/Ce-Al_WI (B) and for 2Ni/Ce-Al_PPT(A,B). In contrast, all the catalysts exhibit a remarkable decline of the total pore volume and mean pore size after Ni impregnation (except 2Ni/Ce-Al_WI(A)) compared to the parent supports, 2Ni/Al₂O₃ and 2Ni/CeO₂-HS_300 (Table 1, entry 7). This observation can be explained by a partial pore blockage by NiO nanoparticles grown over γ -alumina/ceria after impregnation.

3.1.2. XRD patterns

Fig. 1 plots the XRD patterns of the calcined catalysts at 500 °C. In all cases, neat reflections belonging to γ -alumina (JCPDS 10-0425), CeO₂ (JCPDS 34-0394) and NiAl₂O₄ (JCPDS 65-3102/10-0339) can be identified. In particular, the ceria reflections at 2 θ angles of 28.4° (111), 33.0° (200), 47.4° (220), 56.2° (311), 59.0° (222) and 69.3° (400) can be clearly visualized in the parent supports (Ce-Al_WI and Ce-Al_PPT) and after Ni impregnation for 2Ni/Ce-Al_WI(A,B). In contrast, 2Ni/Ce-Al_PPT(A,B) show less intense reflections, suggesting either a lower crystallinity of the ceria phase, or a better dispersion of ceria over γ -alumina probably due to a partial dissolution during Ni impregnation. This latter hypothesis is supported by the higher S_{BET} and pore volume observed for 2Ni/Ce-Al_PPT(A,B) as well by the broader pore size distribution after Ni impregnation.

A negative shift is observed for the Ce(111) reflection in Ce-Al_WI (–0.22%), which becomes more moderate but detectable for 2Ni/Ce-Al_WI(A) and 2Ni/Ce-Al_WI(B) (–0.10% and –0.06%, respectively). This observation can be explained by a possible incorporation of Ni²⁺ with smaller ion radius ($r_{\text{Ni}^{2+}} = 0.72 \text{ \AA}$) into the surface or subsurface of ceria ($r_{\text{Ce}^{4+}} = 0.92 \text{ \AA}$), but not into the ceria lattice, to form substituted Ni-CeO_x [46,63–66]. The characteristic reflections at 43.5° and 63.0° belonging to the NiO phase are not observed, suggesting a high NiO dispersion over ceria-alumina within the limits of the experimental error. Besides, the

Table 1
Main properties of the different catalysts prepared in this study.

Entry	Catalyst	S _{BET} (m ² g ^{–1})	V _g (cm ³ g ^{–1}) ^a	Pore size (Å) ^b	CeO ₂ particle size (nm) ^c
1	γ -Al ₂ O ₃	150	0.528	98.8	–
2	2Ni/Al ₂ O ₃	148	0.504	96.5	–
3	CeO ₂ -HS_300 ^d	236	0.201	32.3	10
4	2Ni/CeO ₂ -HS_300	–	–	–	–
5	Ce-Al_WI	134	0.407	93.5	6.5
6	2Ni/Ce-Al_WI(B)	135	0.374	90.2	6.4
7	2Ni/Ce-Al_WI(A)	127	0.382	94.2	7.0
8	Ce-Al_PPT	146	0.505	100.1	9.0
9	2Ni/Ce-Al_PPT(B)	148	0.461	99.0	3.0
10	2Ni/Ce-Al_PPT(A)	146	0.463	97.4	3.6

^a From BJH desorption branch.

^b From adsorption branch.

^c From XRD at 2 θ = 28.5° (111).

^d CeO₂-HS pre-calcined at 300 °C.

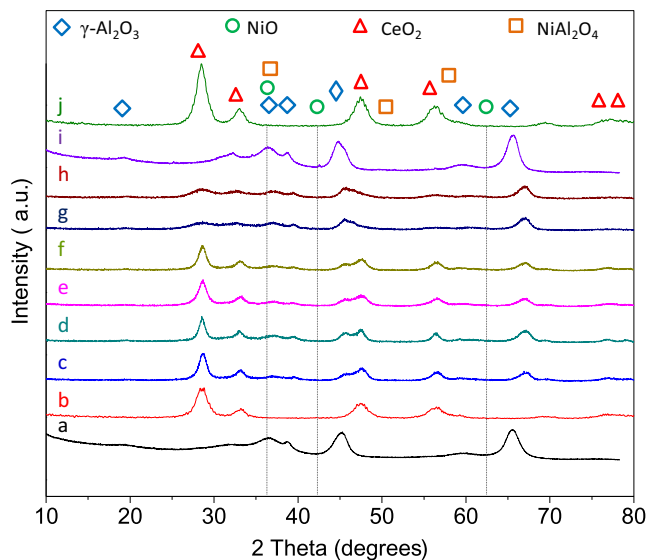


Fig. 1. XRD patterns of Ni/Ce-Al catalysts: (a) γ -Al₂O₃, (b) CeO₂-HS_300, (c) Ce-AL_WI, (d) Ce-AL_PPT, (e) 2Ni/Ce-AL_WI(B), (f) 2Ni/Ce-AL_WI(A), (g) 2Ni/Ce-AL_PPT(B), (h) 2Ni/Ce-AL_PPT(A), (i) 2Ni/Al₂O₃ and (j) 2Ni/CeO₂-HS_300.

reflections belonging to NiAl₂O₄ are hardly distinguishable from γ -Al₂O₃ due to overlapping.

Table 1 lists the CeO₂ (111) crystallite sizes estimated from the Scherrer equation at $2\theta = 28.4^\circ$. The CeO₂ crystallite size is about 6.5 nm and 9.0 nm for Ce-AL_WI and Ce-AL_PPT, respectively. The CeO₂ crystallite size keeps almost unchanged after Ni impregnation for 2Ni/Ce-AL_WI(B) (i.e. before calcination) with an average size about 6.4 nm, whereas a slight increase is observed for 2Ni/Ce-AL_WI(A) with an average particle size about 7 nm. This increase is probably related to partial sintering of ceria nanoparticles when contacting the support with the Ni precursor solution followed by calcination. Opposing this observation and irrespective of the Ni impregnation mode, the Ni/Ce-AL_PPT(A,B) catalysts exhibit a remarkable decrease of the ceria crystallite size down to 3 nm, suggesting a higher dispersion of ceria upon Ni impregnation.

3.1.3. DRUV-Vis

The chemical states of the Ni-supported catalysts and the parent supports (i.e. γ -Al₂O₃, CeO₂-HS_300, Ce-AL_WI and Ce-AL_PPT) were assessed by DRUV-Vis. Fig. 2 plots the corresponding spectra. The γ -alumina support exhibits a distinct band at 280 nm (profile a), while CeO₂-HS_300 exhibits two bands (profile b): (1) a band centered at 320 nm corresponding to O²⁻ → Ce⁴⁺ charge transfer, and (2) a band near 350 nm that can be assigned to inter-band transitions [67,68]. The position of the adsorption edge is observed at about 400–450 nm. No adsorption band at 255 nm corresponding to O²⁻ → Ce³⁺ charge transfer is observed. Ce-AL_WI and Ce-AL_PPT exhibit similar spectra compared to CeO₂-HS_300 (profiles e and f, respectively), but with a blue shift of the adsorption edge from 400 nm to 360 nm as compared to CeO₂-HS_300. However, this shift is more pronounced for the former support (Ce-AL_WI), also showing a decrease in intensity, which can be most likely attributed to a smaller crystallite size of ceria for Ce-AL_WI (6.5 nm) compared to Ce-AL_PPT (9.0 nm) (Table 1). This hypothesis is supported by the study reported by Bensalem et al. [60,69], where an absorbance occurring at ≤ 375 nm may imply the presence of finer ceria crystallites and the shift can be explained by a prevailing presence of Ce⁴⁺-oxygen charge transfer occurring on lower-coordinated Ce⁴⁺ ions.

Concentrating our attention now to the control catalysts, the 2Ni/Al₂O₃ catalyst exhibits distinct absorption bands in the lower

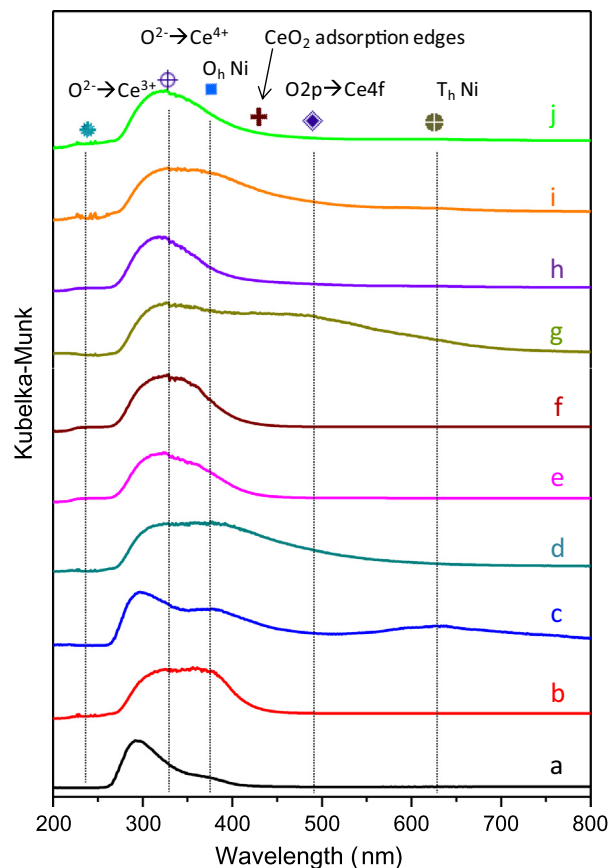


Fig. 2. DRUV-Vis spectra of different catalysts: (a) γ -Al₂O₃, (b) CeO₂-HS_300, (c) 2Ni/Al₂O₃, (d) 2Ni/CeO₂-HS_300, (e) Ce-AL_WI, (f) Ce-AL_PPT, (g) 2Ni/Ce-AL_WI(B), (h) 2Ni/Ce-AL_WI(A), (i) 2Ni/Ce-AL_PPT(B) and (j) 2Ni/Ce-AL_PPT(A).

and higher wavelength regions (profile c). The band at 380 nm can be assigned to a d-d transition for octahedrally (O_h) coordinated Ni in the NiO lattice, while the band appearing at higher wavelength (600–650 nm) can be assigned to a d-d transition for tetrahedrally coordinated (T_h) Ni in the Ni-aluminate spinel. 2Ni/CeO₂-HS_300 (profile d) exhibits a charge transfer band at ca. 320 nm and a broader band in the range 350–450 nm that can be assigned to a d-d transition for O_h-coordinated Ni and to the inter-band transition of ceria, respectively. The adsorption edge is observed at about 500 nm, falling into the visible range. This catalyst also shows a weak broad band in the UV region (<230 nm), which can be attributed to O²⁻ → Ce³⁺ charge transfer. This band is also observed for 2Ni/Ce-AL_WI(B) (profile g), but with weaker intensity and a promoted adsorption edge at 635 nm. In contrast, the spectrum of 2Ni/Ce-AL_WI(A) (profile h) is very similar to that of the bare support (profile e) with an adsorption end at about 380 nm.

The spectra of 2Ni/Ce-AL_WI(A,B) and 2Ni/Ce-AL_PPT(A,B) (profiles g, h and i, j respectively) differ from those of the parent oxides and are strongly affected by the Ni impregnation mode. For example, 2Ni/Ce-AL_WI(B) exhibits three bands: (1) a weak band at 220 nm corresponding to O²⁻ → Ce³⁺ charge transfer, (2) a band at 320 nm being attributed to O²⁻ → Ce⁴⁺ charge transfer, and (3) a broad d-d transition band in the range 400–550 nm being indicative of O_h-coordinated Ni in NiO or due to O 2p → Ce 4f charge transfer transitions. The broadening of this band could also be indicative of a higher density of surface defects for this catalyst [70,71]. Notably, the latter band is only observed for 2Ni/Ce-AL_WI(B), but vanishes from the Ni/Ce-AL_WI(B) catalysts prepared

with lower (0.5 wt%) and higher (8 wt%) Ni loadings (Fig. S4). In the case of 2Ni/Ce-Al_WI(A), the DRUV-Vis spectrum does not show any band in the lower wavelength region (<300 nm) and in the range 400–450 nm, suggesting a weaker Ni-Ce interaction. Finally, none of the Ni-impregnated catalysts (Fig. 2, profiles g–j) show a band in the 600–650 nm region ascribed to Ni aluminates as in the case of 2Ni/Al₂O₃, suggesting a potential role of ceria as barrier between Ni and alumina.

3.1.4. Reducibility of the catalysts

Fig. 3 plots the H₂-TPR profile of 2Ni/Ce-Al_WI and 2Ni/Ce-Al_PPT until 1000 °C, as well as the corresponding profiles for the Ce-Al_WI and Ce-Al_PPT supports, and the benchmark 2Ni/CeO₂-HS_300 and 2Ni/Al₂O₃. Ce-Al_PPT (profile a) displays two bands with different intensities centered at 470 °C and 648 °C that can be ascribed to the reduction of surface and bulk ceria, respectively [72,73]. Upon Ni impregnation, Ni/Ce-Al_PPT shows three major bands (profiles b and c): (1) a first band centered at 160–200 °C corresponding to the reduction of Ni₂O₃ and to a possible reduction of oxygen species generated upon dissolution of Ni²⁺ into the ceria surface or subsurface [74–77]; (2) a second band at 550–650 °C ascribed to the reduction of surface NiO species (β_1 and β_2) interacting with γ -Al₂O₃ [55–57,78,79]; and (3) a third band at T > 700 °C corresponding to the reduction of bulk NiAl₂O₄ spinel in strong interaction with surface alumina [40,45,55–57,79]. The latter band is also present at a much higher intensity for the 2Ni/Al₂O₃ control catalyst (profile g). Finally, no band at T > 850 °C ascribed to CeAlO₃ species is observed for Ni/Ce-Al_PPT catalysts. Opposing these observations, 2Ni/CeO₂-HS_300 (profile h) shows a different reduction profile being characterized by four major bands: (1) two bands centered at 165 °C and 208 °C corresponding

to the reduction of two different NiO species, (2) a third band appearing in the range 300–450 °C that can be ascribed to the reduction of surface ceria, and (3) a fourth band centered at T > 700 °C corresponding to the reduction of bulk ceria.

When the mixed oxides are prepared by the WI method, Ce-Al_WI (Fig. 3, profile d) exhibits a relatively different reduction profile compared to Ce-Al_PPT. Ce-Al_WI shows the presence of two main bands centered at 450 °C and a smaller band at a temperature >850 °C that can be assigned to the reduction of surface ceria [72], and to Ce⁴⁺ → Ce³⁺ reduction into CeAlO₃ [44,80,81]. No evidence of bulk ceria reduction is observed. Upon Ni impregnation, the 2Ni/Ce-Al_WI catalysts (profiles e and f) display five reduction bands: (1) a small band centered at 275 °C that can be ascribed to Ni₂O₃ reduction or to the reduction of oxygen species generated from a Ni-O-Ce solid solution [82–84]; (2) a band at ca. 450 °C corresponding to the reduction of surface ceria; (3) a broad band in the range 550–700 °C being ascribed to the reduction of surface Ni species (β_1 and β_2) interacting with γ -Al₂O₃; (4) a band in the range 730–850 °C corresponding to the reduction of Ni aluminate spinel species (NiAl₂O₄); and (5) a band appearing at very high temperature (>850 °C) that can be attributed to Ce⁴⁺ → Ce³⁺ reduction encompassing CeAlO₃ formation. Note that the reduction of surface Ni species occurs at lower temperature for 2Ni/Ce-Al_WI (B) than for 2Ni/Ce-Al_WI(A) (645 °C instead of 665 °C). Altogether, the results confirm that the reducibility of surface Ni species depends to an important extent on the Ni impregnation mode.

The appearance of a reduction band ascribed to CeAlO₃ irrespective of the presence of Ni may inform about the particle size of CeO_{2-x} crystallites in the catalysts. As outlined by Kaufherr et al. [85], the formation of CeAlO₃ depends on the reduction temperature, which is governed by the average particle size of ceria. As a rule, a higher reduction temperature is required for larger ceria particles to favor Ce diffusion into alumina to generate a solid solution. In our case, the reduction temperature for CeAlO₃ formation decreases from 870 °C for Ce-Al_WI to 865 °C for 2Ni/Ce-Al_WI (B), while it increases to 880 °C for 2Ni/Ce-Al_WI(A). This observation can be interpreted by the presence of smaller dispersed ceria particles in 2Ni/Ce-Al_WI(B), favoring its reducibility and accordingly the formation of surface Ni species (β type).

The H₂-TPR study was further extended to Ni/Ce-Al_WI catalysts with variable Ni loading (0.5–8 wt%) (Fig. S5). The reduction profile of a very low Ni-loaded catalyst (0.5Ni/Ce-Al_WI) is very similar to that observed for the parent Ce-Al_WI (Fig. 3, profile d). In contrast, the catalyst displaying the highest Ni loading (8Ni/Ce-Al_WI) exhibits a major band in the temperature range 500–700 °C corresponding to the reduction of surface Ni (β_1 and β_2 type), as well as to minor bands at 747 °C and 850 °C attributed to NiAl₂O₄ and CeAlO₃, respectively. Unlike 2Ni/Ce-Al_WI, the reduction bands corresponding to surface Ni species and NiAl₂O₄ shift to lower temperature at higher Ni loading, indicating weaker Ni-alumina interactions. Interestingly, the intensity of the band at 874 °C is lower for 8Ni/Ce-Al_WI(B), which could be probably due to a higher surface occupancy by Ni instead of ceria, and thus to a lower degree of interaction between alumina and ceria.

3.2. Catalytic results

3.2.1. Amination of benzyl alcohol with aniline

The Ni/Ce-Al catalysts were first tested in the model amination reaction of benzyl alcohol with aniline at 160 °C for 3 h using 65 mg of catalyst pre-reduced at 580 °C for 30 min. Fig. 4 plots the results obtained for the different catalysts, as well for the benchmark 2Ni/Al₂O₃ and 2Ni/CeO₂_300, while a complete list is provided in Table S1 including control catalysts. The parent supports (Ce-Al_WI and Ce-Al_PPT) display very low activity (~10% aniline conversion) with formation of BZIA as major product.

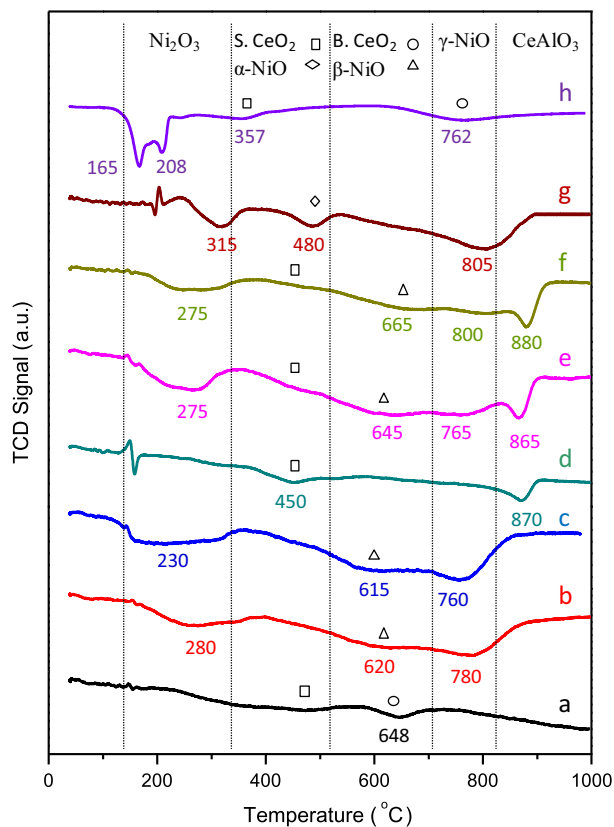


Fig. 3. H₂-TPR profiles of Ni/Ce-Al catalysts synthesized by the wet impregnation method: (a) Ce-Al_PPT, (b) 2Ni/Ce-Al_PPT(B), (c) 2Ni/Ce-Al_PPT(A), (d) Ce-Al_WI, (e) 2Ni/Ce-Al_WI(B), (f) 2Ni/Ce-Al_WI(A), (g) 2Ni/Al₂O₃, and (h) 2Ni/CeO₂-HS_300.

Among the Ni-impregnated catalysts, 2Ni/CeO₂-HS_300 exhibit the highest activity with 28% aniline conversion and 68% BZA selectivity. Among the different 2Ni/Ce-Al catalysts, 2Ni/Ce-Al_WI(B) shows the highest activity with ~70% aniline conversion and 88% BZA selectivity. In contrast, 2Ni/Ce-Al_WI(A) displays a lower activity (23% aniline conversion and 43% BZA selectivity) with BZIA as major product with 56% selectivity. The opposite trend (i.e. a higher activity) is observed for 2Ni/Ce-Al_PPT(A) synthesized by the precipitation method and for which Ni was impregnated after calcination.

To survey the effect of the reduction temperature on the catalytic activity for amination, the best performing catalyst, i.e. 2Ni/Ce-Al_WI(B), was reduced at different temperatures in the range 400–800 °C and the activity for benzyl alcohol amination was further measured (Table S1). The reduction at lower temperature (400 °C) results into a lower activity with an aniline conversion of ~10% towards BZIA. A similar effect is observed at very high reduction temperatures (800 °C) with only 18% aniline conversion and 44% BZA selectivity. Opposing these results, a reduction of temperature 580 °C affords a high aniline conversion (70%) and BZA selectivity (88%).

The above stated activity trends as a function of the reduction temperature can be explained on the basis of the H₂-TPR profile of 2Ni/Ce-Al_WI(B) (Fig. 3, profile e). When the catalyst is reduced at 400 °C, only Ni₂O₃ species are expected to be reduced to Ni, resulting in a very low activity. In contrast, when the catalyst is reduced by 600 °C, other Ni species are expected to come into act, encompassing mainly bulk Ni species (200–300 °C), reduced surface ceria species (400–500 °C) and surface Ni species (500–600 °C). The presence of surface Ni species after reduction at 600 °C, probably interacting with surface ceria and alumina, appears to be a main driver for enhancing the catalytic activity. Finally, the catalyst reduced at 800 °C shows the preferential reduction of bulk ceria and Ni aluminate species, which are not active for catalysis. Hence, it can be concluded that a reduction temperature about 600 °C is compulsory for favoring the formation of surface Ni species, which can help achieving a better reducibility and controlled Ni-Ce or Ni-Al interactions. Accordingly, this reduction temperature was used in the remainder of this study to assess the performance of the different 2Ni/Ce-Al catalysts for *n*-octanol amination with ammonia.

3.2.2. Amination of *n*-octanol with ammonia

3.2.2.1. Catalytic properties of Ni/Ce-Al catalysts. Fig. 5 plots the performance of the different 2Ni/Ce-Al catalysts for *n*-octanol amination with ammonia at 180 °C for 4 h after pre-reduction at 580 °C, as well as for different benchmark catalysts, whereas Table S2

compiles the results obtained. The parent supports without metal do not display any activity, as previously observed in the model reaction. Among the Ni-impregnated catalysts, 2Ni/CeO₂-HS_300 shows activity with 32% *n*-octanol conversion and 79% of OA selectivity. The Ni/Ce-Al catalysts are very active for *n*-octanol amination compared to 2Ni/Al₂O₃. Among the different catalysts, those synthesized by the wet impregnation method and displaying a high density of β-type Ni species (i.e. 2Ni/Ce-Al_WI) exhibit higher activities. The Ni impregnation mode impacts the catalytic properties with 2Ni/Ce-Al_WI(B) impregnated just before calcination showing a higher activity (27% *n*-octanol conversion, 78% OA selectivity). This trend opposes to that observed for the catalysts prepared by co-precipitation: while 2Ni/Ce-Al_PPT(B) displays no activity, 2Ni/Ce-Al_PPT(A) exhibits 23% *n*-octanol conversion and 77% OA selectivity.

3.2.2.2. Effect of the catalyst loading and reaction time. The catalytic performance of 2Ni/Ce-Al_WI (B) was further optimized by tuning the loading and the reaction time (Fig. 6). An increase of the catalyst weight from 65 mg to 235 mg (5 mol%) while keeping the reaction time constant (4 h) results in an enhancement of the *n*-octanol conversion to 64% with an OA selectivity of 80% (46% OA yield). Furthermore, at a constant catalyst loading of 65 mg, an increase of the reaction time from 4 h to 24 h also results in a remarkable increase of the *n*-octanol conversion and OA selectivity to 55% and 94% after 24 h (43% OA yield), respectively. An increase of the catalyst loading from 65 mg to 110 mg at a reaction time of 24 h results in an increase of the *n*-octanol conversion and OA selectivity to 94% and 78% (60% OA yield), respectively.

Finally, a series of Ni/Ce-Al_WI(B) catalysts with variable Ni loading were prepared and tested for *n*-octanol amination with ammonia at 24 h using 65 mg of catalyst. No activity is observed for the catalyst with the lowest Ni loading i.e. 0.5Ni/Ce-Al_WI(B), while 8Ni/Ce-Al_WI(B) affords almost full *n*-octanol conversion in favor of DOI (47% selectivity) with an OA yield of only 20%. This body of results clearly point out the benefits of 2Ni/Ce-Al_WI(B) over the other formulations prepared in this study for enhancing the catalytic activity towards OA.

3.2.2.3. Catalytic properties of 2Ni/Ce-Al_WI(B) compared to 8Ni/Al₂O₃. In a further step of our study, we compared the catalytic properties of 2Ni/Ce-Al_WI(B) against the benchmark 8Ni/Al₂O₃ also prepared by the IWI method in the amination of *n*-octanol reaction with ammonia. Interestingly, when representing the OA selectivity vs. *n*-octanol conversion, an almost constant trend is observed for 2Ni/Ce-Al_WI(B), whereas a decreasing trend is observed for 8Ni/Al₂O₃ (Fig. 7). The best performance for 8Ni/Al₂O₃ towards OA

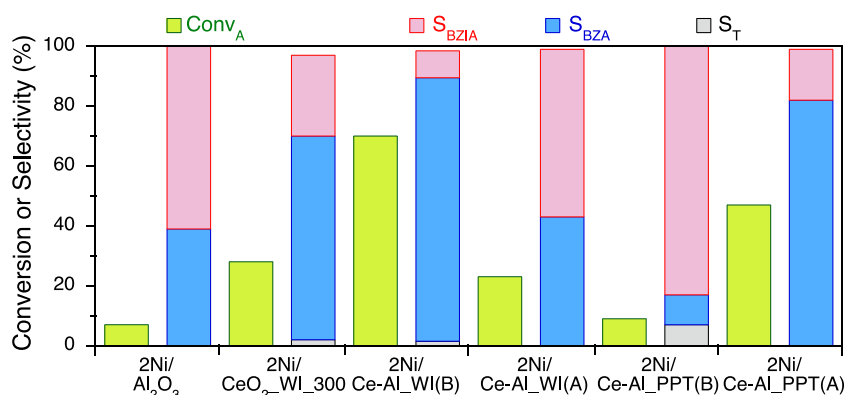


Fig. 4. Performance of 2Ni/Ce-Al catalysts in the amination reaction of benzyl alcohol with aniline. Reaction conditions: Aniline- 2 mmol, Benzyl alcohol- 6 mmol, T- 160 °C, Time- 3 h, Cat- 65 mg, no solvent, rpm- 600, Ar atm.

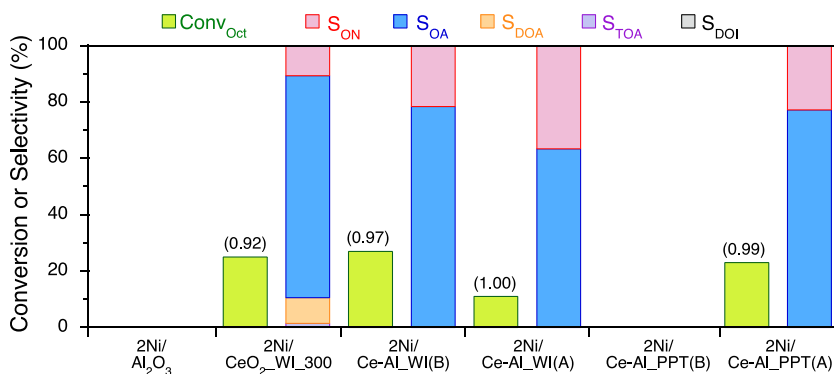


Fig. 5. Performance of 2Ni/Ce-Al catalysts in the amination reaction of *n*-octanol with ammonia. The numbers in parentheses indicate the carbon balance. Reaction conditions: Oct- 1.3 mmol, NH₃- 7 bar, T- 180 °C, Time- 4 h, Cat- 65 mg, Solvent- 3 mL *o*-xylene, rpm- 600.

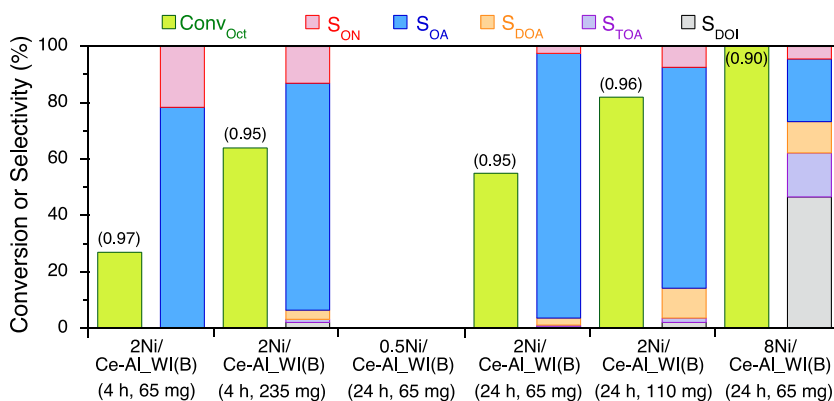


Fig. 6. Performance of Ni/Ce-Al_{WI}(B) catalysts in the amination reaction of *n*-octanol with ammonia. The numbers in parentheses indicate the carbon balance. Other reaction conditions as in Fig. 5.

encompasses 83% *n*-octanol conversion and 73% OA selectivity (54% OA yield) after 4 h. An increase of the reaction time results in a decrease of the OA selectivity in favor of the secondary amine (DOA). Moreover, when comparing the turnover number (TON) for 2Ni/Ce-Al_{WI}(B) and the corresponding TON for 8Ni/Al₂O₃ after 24 h, the former catalyst outstands the benchmark catalyst (Table 2). Also noteworthy, the TON achieved for 2Ni/Ce-Al_{WI}(B) after 24 h compares well with the TON reported by Shimizu et al. [23] over 10Ni/θ-Al₂O₃ catalyst (TON = ~85 at 160 °C for 13 h), even if the Ni loading used here is seven times smaller (1.4 mol%Ni vs. 5 mol%Ni). In other words, 2Ni/Ce-Al_{WI}(B) affords a save about ~75% of Ni metal for achieving a comparable OA yield (60%) due to a higher Ni dispersion in the form of β-species. In addition to these benefits, 2Ni/Ce-Al_{WI}(B) affords a much better carbon balance (95% vs. 85%).

3.3. Understanding the structure and catalytic behavior of 2Ni/Ce-Al_{WI}

The catalytic results for the model and *n*-octanol amination reactions presented above reveal an enhanced activity for the catalysts prepared by wet impregnation (2Ni/Ce-Al_{WI}) instead of the precipitation method (2Ni/Ce-Al_{PPT}). In light of these results, we explored in more detail the structure of 2Ni/Ce-Al_{WI} before and after reaction along with control catalysts.

The elemental composition of 2Ni/Ce-Al_{WI}(A,B) was confirmed by ICP-OES. The Ni and Ce loading was found to be very near to the nominal values. As a matter of example, the Ni and Ce loading estimated for both catalysts is 1.7 wt% and 15 wt%, respec-

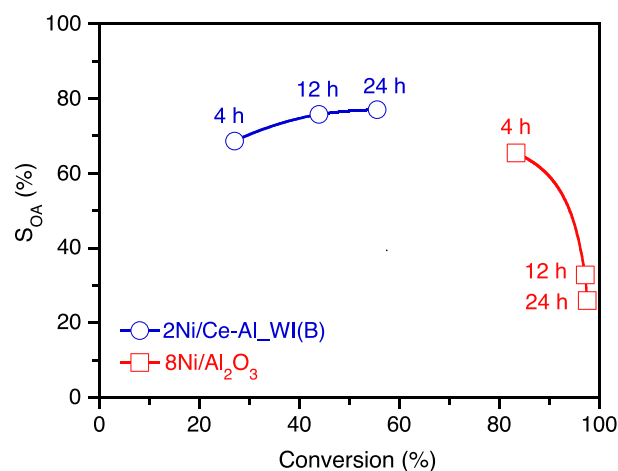


Fig. 7. Evolution of the OA selectivity vs. *n*-octanol conversion for 2Ni/Ce-Al_{WI}(B) and 8Ni/Al₂O₃ as a function of the reaction time. Other reaction conditions as in Fig. 5.

tively, for 2Ni/Ce-Al_{WI}(B), and 1.8 wt% and 15 wt%, respectively, for 2Ni/Ce-Al_{WI}(A). The morphology of 2Ni/Ce-Al_{WI}(B) was inspected by SEM combined with EDS analysis (Figs. S6–S8, Table S3). The SEM micrographs show the presence of spherical γ-Al₂O₃ particles with a size in the range of 40–90 μm. The Ce and Ni loadings show values at ca. 15 wt% and 1.8–2.3 wt% matching the theoretical loadings measured from ICP-OES analysis. A

very homogeneous Ni distribution is observed for 2Ni/Ce-Al_WI(B) (Fig. S8).

Fig. 8 plots the XPS spectra for the Ce 3 d, Ni 2 p and O 1s core levels for 2Ni/Ce-Al_WI(B) and 2Ni/Ce-Al_WI(A) and the corresponding deconvolution after pre-reduction, whereas Table 3 summarizes the surface concentrations measured for Ce, Al and Ni in the calcined and reduced states. The deconvoluted Ce 3 d core-level spectra could be assigned to eight spin-orbit coupling levels corresponding to the $3d_{5/2}$ (v) and $3d_{3/2}$ (u) states (Fig. 8a and d). The v components show binding energies (BE) at 882.7 eV (v), 884.1 eV (v'), 888.5 eV (v'') and 898.3 eV (v'''), while the u components show BEs at 901.3 eV (u), 903.4 eV (u'), 907.3 eV (u'') and 917.0 eV (u''') [61,86,87]. Noteworthy, the lack of increase of the BE for the v components in the presence of Ni compared to the value commonly accepted for ceria suggests very low Ni incorporation in the ceria surface or subsurface [63–66]. Furthermore, the presence of v' and u' components combined with the presence of large bands for v''' and u''' components indicates the presence of Ce^{3+} in the surface of ceria, but without generating $CeAlO_3$ [81]. The proportion of Ce^{3+} can be estimated at ca. 40% for both 2Ni/Ce-Al_WI(B) and 2Ni/Ce-Al_WI(A), as inferred from Eq. (1) implemented with the integrated areas for the v and u components in the Ce 3d spectra (Table 3, column 9). Besides, the Ce/Al molar ratio is higher for 2Ni/Ce-Al_WI(B) than for 2Ni/Ce-Al_WI(A) both in the calcined (0.059 vs. 0.027) and pre-reduced catalysts (0.039 vs. 0.028) (Table 3, column 5 and 8), suggesting a higher proportion of ceria on the catalyst surface for 2Ni/Ce-Al_WI(B).

The Ni $2p_{3/2}$ spectra for the pre-reduced 2Ni/Ce-Al_WI(B) and 2Ni/Ce-Al_WI(A) exhibit two main bands centered at 856.5 eV and 856.8 eV that are indicative of the presence of Ni^{2+}

(Fig. 8b and e). Moreover, 2Ni/Ce-Al_WI(A) displays an additional small band centered at 852.0 eV that can be ascribed to Ni^0 (5%), along with a band at ~ 861 eV that can be assigned to a shake-up satellite band of NiO or Ni_2O_3 [88,89]. The absence of band corresponding to reduced Ni species in 2Ni/Ce-Al_WI(B) might be ascribed to the formation of a Ni-O-Ce solid solution on the ceria surface or subsurface, even after pre-reduction. This hypothesis can be supported by the low Ni/Ce molar ratio approaching 0.5 for this sample (Table 3, column 6), favoring Ni-Ce interaction [63,90].

The XPS spectra for the O 1s core level of 2Ni/Ce-Al_WI(B) and 2Ni/Ce-Al_WI(A) (Fig. 8c and f) show the presence of a major band centered at 531.5 eV that agrees well with the BE of lattice O in the alumina phase. In addition, a shoulder band centered at 533 eV can be observed, matching the band commonly observed for pure ceria accounting for weakly bounded oxygen (e.g., hydroxyl groups, vacancies) (Fig. S9b). No band is observed at about 529–530 eV belonging to lattice O in pure ceria, suggesting an increase by 2 eV of the BE compared to pure ceria. Such an increase has already been described in highly dispersed ceria in CeO_2-SiO_2 composites [61], and can be attributed to a change in the coordination environment of ceria, favoring its interaction with Al_2O_3 by the formation of Ce-O-Al bonds. Furthermore, the formation of O-ion vacancies in the subsurface layer of ceria due to partial incorporation of Ni^{2+} cannot be ruled out [91–93]. Finally, when we compare the relative areas for the O1s bands in 2Ni/CeO₂-HS_300, 2Ni/Al₂O₃, 2Ni/Ce-Al_WI(B) and 2Ni/Ce-Al_WI(A) (Fig. S9e), the area for 2Ni/Ce-Al_WI(A) is very similar to that of 2Ni/Al₂O₃. Also, the area for the O1s band in 2Ni/Ce-Al_WI(B) is closer to that of 2Ni/CeO₂-HS_300. These

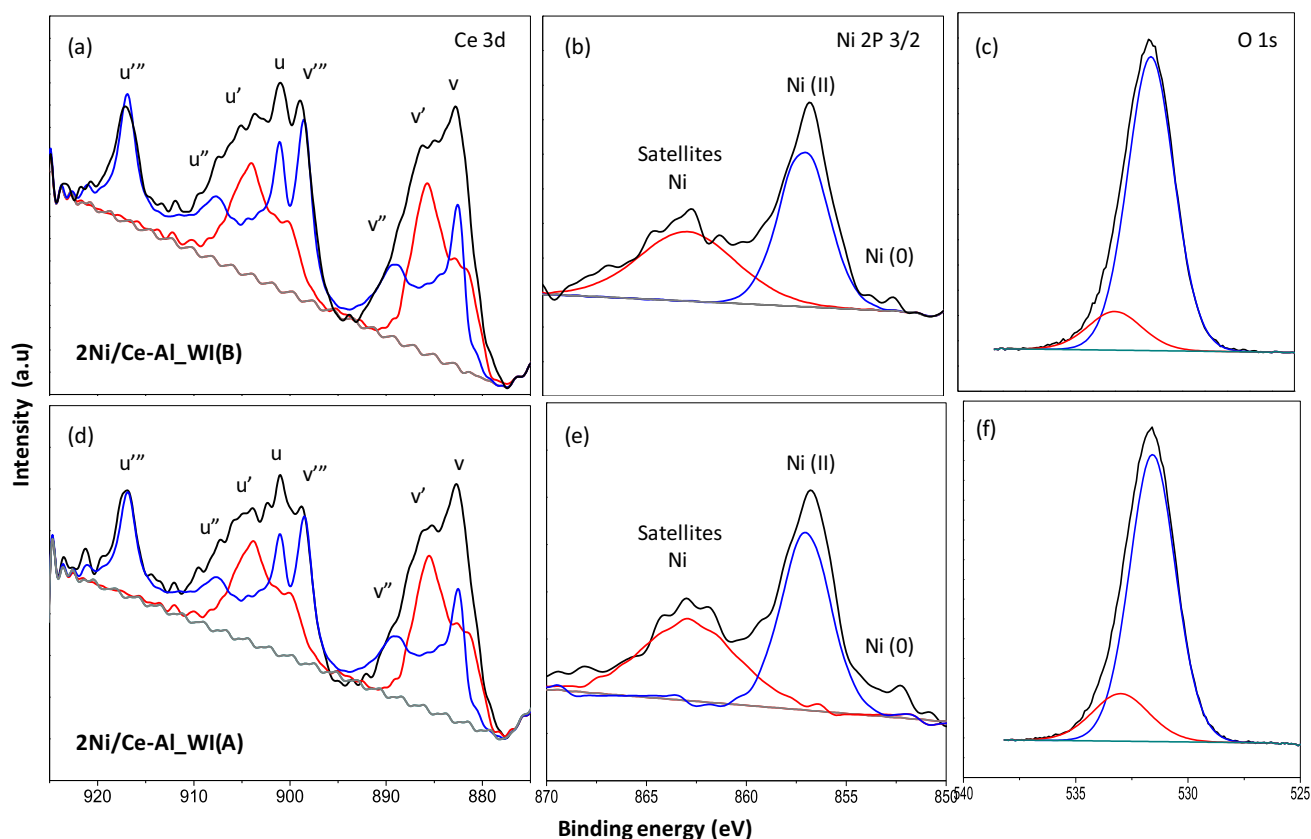


Fig. 8. XP spectra of Ni/Ce-Al_WI(B) and Ni/Ce-Al_WI(A) for the Ce 3 d (a), Ni 2p (b) and O 1s (c) core levels. The samples were pre-reduced at 580 °C for 30 min under H_2 flow before the XPS analyses.

Table 2Comparison between the performance of 2Ni/Ce-Al_WI(B) and Al₂O₃-supported Ni catalysts for the direct amination of *n*-octanol with ammonia.^a

Entry	Catalyst	%D ^b	Loading (mol%)	%Octanol Conv ^c	%Selectivity ^d					%Yield	TON ^e	Carbon balance
					ON	OA	DOA	TOA	DOI			
1	2Ni/Ce-Al_WI(B)	35	1.4	55	2.4	94	2.4	0.6	0.6	43	85	95
2	2Ni/Ce-Al_WI(B)	35	2.3	82	7.4	78	11	1.6	2.0	60	69	96
3	8Ni/Al ₂ O ₃ ^f	15	6	83	10.1	73	16	0.7	–	54	54	95
4	8Ni/Al ₂ O ₃	15	6	97	5.4	28	66	–	–	25	25	96
6	10Ni/θ-Al ₂ O ₃ ^g	16	5	90	–	91	9.3	–	–	70	83	85

^a Reaction conditions: Oct- 1.3 mmol, NH₃- 7 bar, T- 180 °C, Time- 24 h, Solvent- 3 mL *o*-xylene, rpm- 600.^b Dispersion calculated from CO-TPD considering Ni/CO, S.F. = 2.^c Estimated from GC.^d Normalized selectivity.^e TON: moles of OA formed per moles of surface Ni at 24 h.^f Reaction time: 4 h.^g Reaction conditions: Oct- 3 mmol, NH₃- 4 bar, T- 160 °C, Time- 13 h, Solvent -4 mL *o*-xylene (Ref. [23]).**Table 3**

Composition of 2Ni/Ce-Al_WI catalysts measured by XPS.

Entry	Catalyst	Calcined catalysts			Reduced catalysts ^a			
		Ni/Ce	Ni/Al	Ce/Al	Ni/Ce	Ni/Al	Ce/Al	Ce ³⁺ %
1	2Ni/Al ₂ O ₃	–	0.046	–	–	0.026	–	–
2	2Ni/Ce-Al_WI(B)	0.767	0.045	0.059	0.547	0.022	0.039	40
3	2Ni/Ce-Al_WI(A)	1.648	0.044	0.027	1.142	0.032	0.028	40

^a Catalysts pre-reduced under at 580 °C for 30 min under H₂ flow.

observations suggest a higher oxygen contribution from CeO₂ to the Al₂O₃ lattice in 2Ni/Ce-Al_WI(B).

Fig. 9 plots the CO-TPD profiles of 2Ni/Ce-Al_WI(B) and 2Ni/Ce-Al_WI(A), as well as the corresponding profiles for the control catalysts, whereas Table S4 lists the corresponding Ni dispersion, average particle size and total amount of CO desorbed from the support and the Ni phase. The bands in the lower temperature region (40–150 °C) are generally attributed to CO desorption from metallic Ni, whereas the bands in the mid-temperature region (200–400 °C) are ascribed to CO desorption from ceria. The remaining high-temperature bands (T > 400 °C) are attributed to CO desorption as CO₂ from Al₂O₃-CeO₂. Noteworthy, unlike 2Ni/Ce-Al_WI(B) and 2Ni/Ce-Al_WI(A), no band in the low-temperature region (~80 °C) is observed for neither γ -alumina nor 2Ni/Al₂O₃,

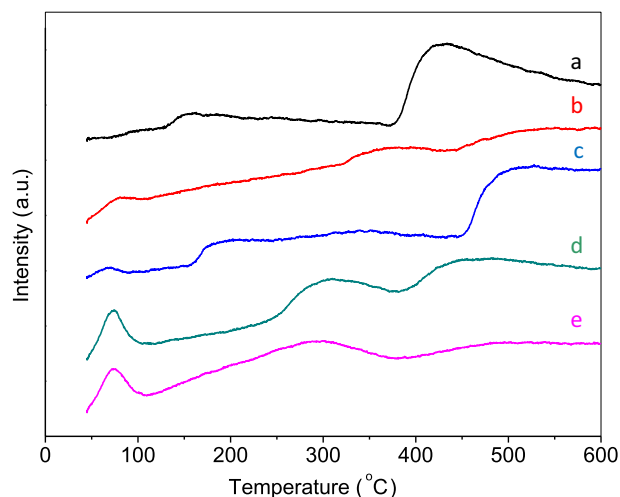


Fig. 9. CO-TPD profiles for Ni/Ce-Al and control catalysts synthesized by the wet impregnation method: (a) γ -Al₂O₃, (b) Ce-Al_WI, (c) 2Ni/Al₂O₃, (d) 2Ni/Ce-Al_WI(B) and (e) 2Ni/Ce-Al_WI(A).

pointing out that only a fraction of Ni is available for interacting with CO in 2Ni/Al₂O₃ after ceria-doping. A higher Ni dispersion (35%) is observed for 2Ni/Ce-Al_WI(B) with a average particle size for Ni of ~2.5 nm, whereas 2Ni/Ce-Al_WI(A) shows a Ni dispersion of 21% with a average particle size of Ni ~4 nm for Ni (Table S4, entries 4 and 5). In addition to a higher Ni dispersion, the genesis of very small Ni nanoparticles over 2Ni/Ce-Al_WI(B) favoring the exposition of edges and corners can also be regarded as a driver for the enhanced catalytic activity on this catalyst for *n*-octanol amination.

A closer inspection to 2Ni/Ce-Al_WI(B) by STEM/EDS (Figs. 10 and 11 and Fig. S10) indicates a distribution of ceria nanoparticles with a size <10 nm supported over alumina arranged in small agglomerates. Ni appears as homogeneously dispersed over alumina (Fig. 12), matching the observations pointed out above using SEM/EDS, but being preferentially located near the ceria nanoparticles. The Ni nanoparticles show non-uniform shape and average particle size in range 2–3 nm, which is in fairly good agreement with the average particle size measured by CO-TPD. This morphology confirms a major role of ceria in assisting Ni dispersion over alumina during impregnation, hampering in turn the formation of aluminates.

From the above characterization and catalytic results, we can conclude that the enhanced catalytic activity of 2Ni/Ce-Al_WI(B) for the production of primary amines from the direct amination reaction of *n*-octanol with ammonia can be attributed to the genesis of small Ni nanoparticles over alumina promoted by small ceria nanoparticles assembled in agglomerates. Furthermore, the Ni-ceria interaction favors the generation of readily reducible surface Ni species, as well as the suppression of inactive Ni aluminates. A plausible structure of 2Ni/Ce-Al_WI(B) is proposed in Fig. 13.

3.4. Recyclability and post-catalytic characterization of 2Ni/Ce-Al_WI(B) catalyst

The recyclability of the catalyst showing best performance (2Ni/Ce-Al_WI(B)) was surveyed in two consecutive cycles. Briefly, after the 1st run, the catalyst was separated by centrifugation, washed

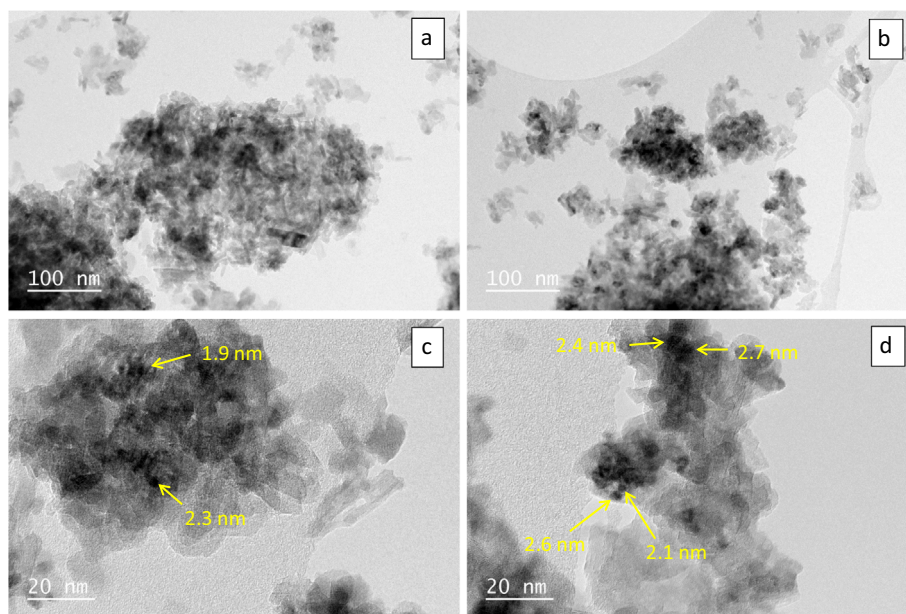


Fig. 10. STEM micrographs of 2Ni/Ce-Al_WI(B). The sample consists of non-uniform Ni nanoparticles with a particle size in the range 2–3 nm: (a) 100 nm, (b) 100 nm, (c) 20 nm and (d) 20 nm.

with ethanol to remove the organic content, dried in an oven and calcined at 500 °C for 6 h. The calcined catalyst was used in a 2nd reaction run after reduction under H₂ at 580 °C for 30 min. Table S5 lists the results obtained for *n*-octanol amination with ammonia at 180 °C for 24 h. The *n*-octanol conversion decreases from 55% after the 1st run to 7% after the 2nd run with only a slight decrease of the OA selectivity from 94% to 82%. A further increase of the reduction temperature to 750 °C for 30 min after the 1st run enhances the *n*-octanol conversion to 13% with decrease in the OA

selectivity to 68% after the 2nd run. This drop in the catalytic activity suggests a modification of the active surface Ni species during the reaction. However, in line with reported studies on low-Ni catalysts [94], no Ni leaching during the 1st run and 2nd run has been observed in our study as confirmed by ICP analysis. In the case of cerium content, a slight decrease is observed from an initial value of 14.8 wt% to 13.8 wt% after the first 1st run.

To rationalize the catalyst evolution during reaction, a part of the spent 2Ni/Ce-Al_WI(B) catalyst after the 1st run was calcined

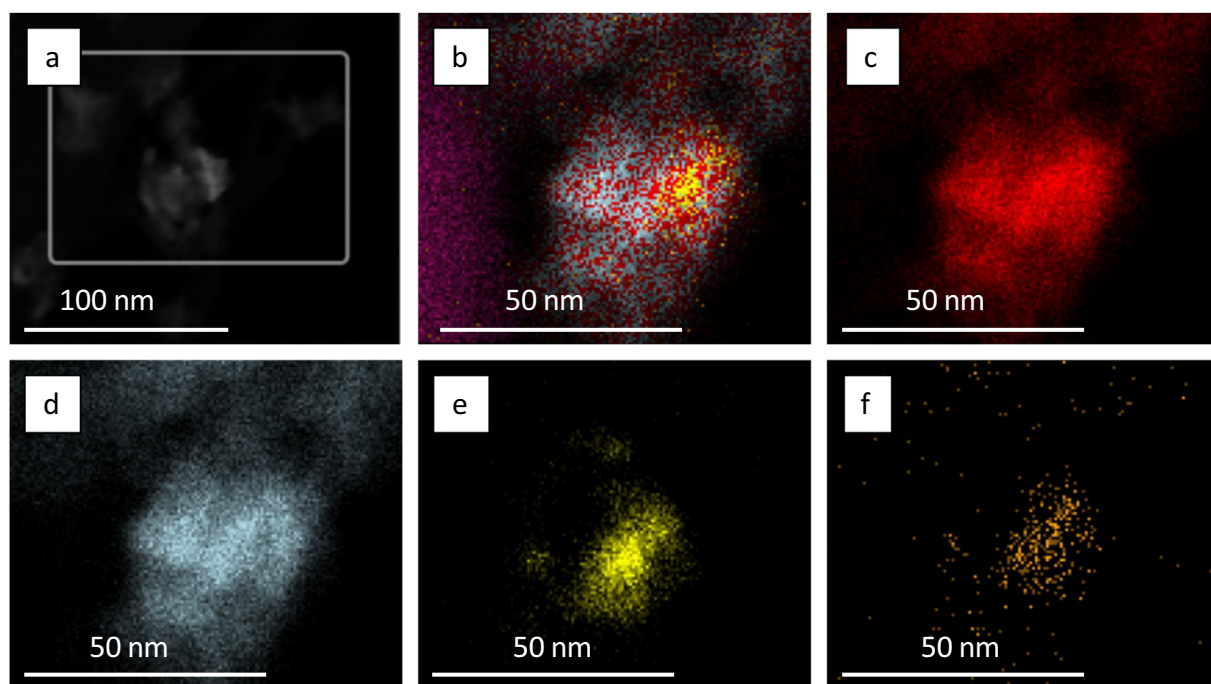


Fig. 11. EDS maps of 2Ni/Ce-Al_WI(B) during STEM analysis: (a) area of EDS map acquisition marked by white rectangle, (b) mixture, (c) O K, (d) Al K, (e) Ce L, and (f) Ni K.

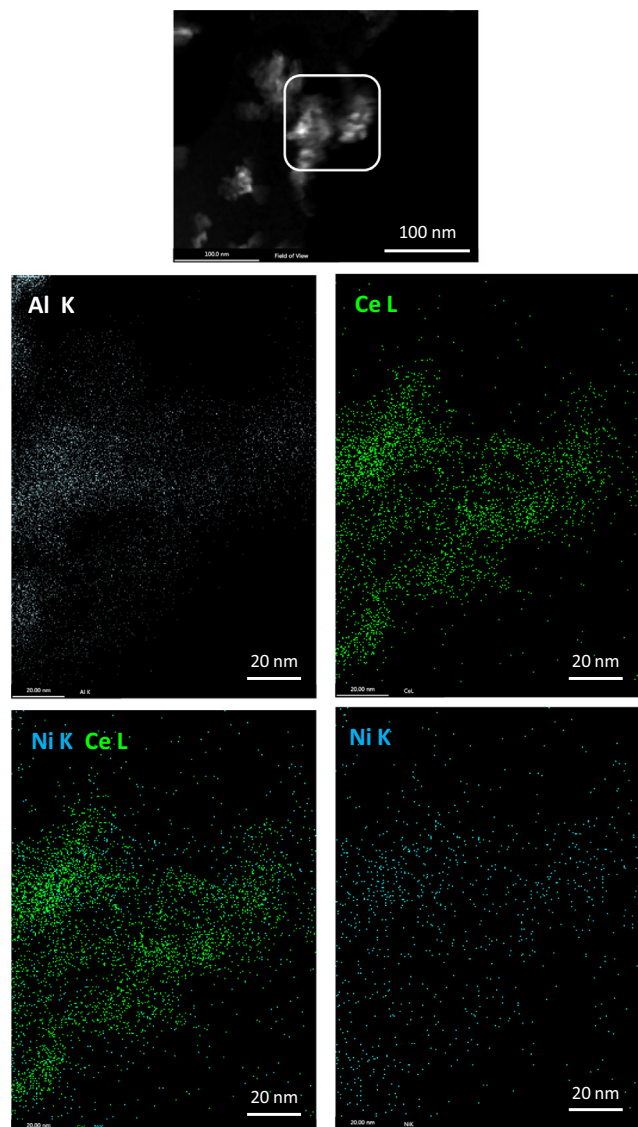


Fig. 12. EDS images of selected area of 2Ni/Ce-Al_WI(B) during STEM analysis showing highly dispersed Ni.

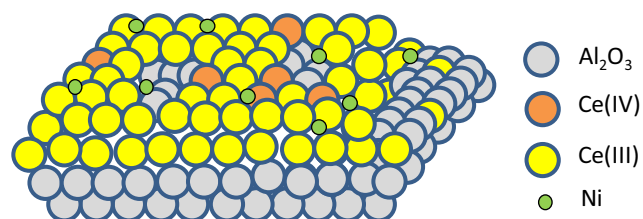


Fig. 13. Proposed structure for 2Ni/Ce-Al_WI(B).

at 500 °C under air flow and subjected to H_2 -TPR analysis to assess its reducibility compared to the fresh catalyst (Fig. 14-left). The spent 2Ni/Ce-Al_WI(B) catalyst shows a similar reduction pattern to that of the fresh catalyst, being characterized by five reduction bands. Nonetheless, the spent catalyst displays a shift to higher temperatures for surface Ni species (β_1 and β_2 type), suggesting the presence of a stronger interaction between Ni and alumina after the 1st run. This observation suggests that, besides the presence of active surface Ni species, the interaction between Ni and

ceria is also relevant for boosting the catalytic activity. The deconvolution of the H_2 -TPR profiles of the fresh and spent catalysts shows a clear demarcation between ceria and Ni in the spent catalyst (Fig. S11). The integrated areas under the individual bands are listed in Table S6. The results show that relative areas of the bands keep almost unchanged. However, the band centered at 441 °C decreases to 396 °C, whereas the band centered at 596 °C shifts to a higher temperature (655 °C).

Fig. 14-right plots the DRUV-Vis spectra of the fresh and spent 2Ni/Ce-Al_WI(B) catalyst calcined at 500 °C under air flow. The original band centered at 320 nm due to $O^{2-} \rightarrow Ce^{4+}$ charge transfer is still visible in the spent catalyst, showing a small shoulder at ~ 380 nm being indicative of the presence of O_h -coordinated Ni in the NiO lattice. Nevertheless, the broad band in the range 450–550 nm present in the fresh catalyst vanishes after reaction, reflecting a change in the coordination environment of Ni and also probably in the density of O vacancies in ceria. Partial incorporation of Ni in the ceria surface or subsurface during reaction is not excluded. The small hump at 640 nm can be ascribed to the presence of T_h -coordinated Ni in $NiAl_2O_4$.

Interestingly, the DRUV-Vis spectrum of the spent 2Ni/Ce-Al_WI(B) (Fig. 14-right, profile b) is very similar to that obtained on the fresh 2Ni/Ce-Al_WI(A) for which Ni-impregnation was performed after calcination (Fig. 14-right, profile c). This observation appears to indicate that the Ni-Ce interaction might disturb the environment of Ni during reaction, or that the spent catalyst might be mainly constituted of only surface Ni as for the fresh 2Ni/Ce-Al_WI(A). Furthermore, when comparing the H_2 -TPR profiles of the spent 2Ni/Ce-Al_WI(B) (Fig. 14-left, b) and the fresh 2Ni/Ce-Al_WI(A) (Fig. 14-left, c), very similar reduction patterns are observed, suggesting a similar Ni speciation. Adding the observation that the catalytic activity of the spent 2Ni/Ce-Al_WI(B) and the fresh 2Ni/Ce-Al_WI(A) are very similar, we can conclude that, after the reaction, 2Ni/Ce-Al_WI(B) has been restructured and behaves in a similar way as the fresh 2Ni/Ce-Al(A).

At last, we investigated coke deposition on 2Ni/Ce-Al_WI(B) after the 1st run using TG analysis. The TG profile of the fresh 2Ni/Ce-Al_WI(B) (Fig. S12, profile a) shows a small weight loss near 100 °C due to water removal. In contrast, the TG profile of the spent catalyst (Fig. S12, profile b) shows two weight loss regions at lower and higher temperatures. The weight loss of 2% near 100 °C can be attributed to physically adsorbed water, whereas the larger weight loss (9%) in the region 300–400 °C can be attributed to the combustion of amorphous carbon (C_x) deposits [95]. This observation indicates that coke is not formed in large amount during *n*-octanol amination with ammonia and that coke can be completely removed from the catalyst after calcination at 400 °C.

4. Conclusions

A series of low-Ni catalytic formulations (2 wt% Ni) supported over Ce-Al mixed oxides achieved an unprecedented activity and selectivity to primary amines in the direct amination reaction of *n*-octanol with ammonia. The addition of ceria as promoter to 2Ni/ Al_2O_3 improved not only the reducibility by generating active Ni surface species, but also promoted the formation of very small nickel nanoparticles (2–3 nm) in detriment of Ni aluminates. However, the properties of the catalysts were strongly dependent on the method of preparation. The best results were achieved on a formulation based on Ce-Al supports prepared by wet impregnation of ceria over alumina followed by incipient wetness impregnation of the Ni precursor solution before calcination. After optimization, this catalyst afforded a comparable activity to the benchmark catalysts, but saving up to 75% Ni. The present study

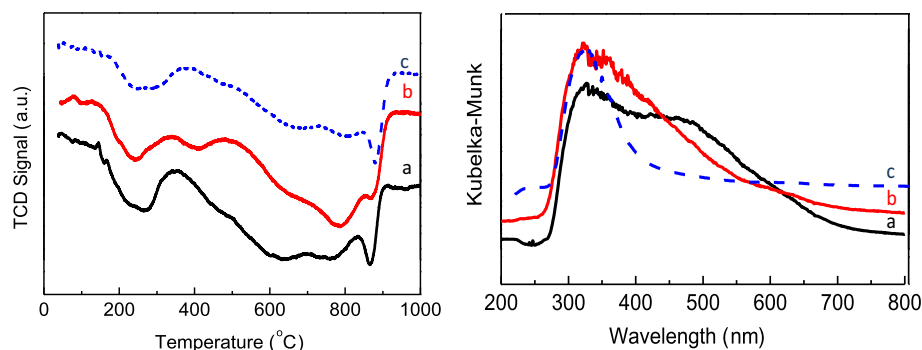


Fig. 14. H₂-TPR profiles (left) and DRUV-Vis spectra (right) of 2Ni/Ce-Al-WI(B) before (a) and after reaction (b), 2Ni/Ce-Al-WI(A) before reaction (c). Reaction conditions: Oct-1.3 mmol, NH₃- 7 bar, T- 180 °C, Time- 24 h, Cat- 65 mg, Solvent- 3 mL o-xylene, rpm- 600.

opens an avenue for further investigations on low-Ni formulations for various catalytic applications.

Acknowledgements

This work was supported by the French Agency of Research (ANR) through the SHAPes program (contract 13-CDII-0004-06). The REALCAT platform is benefiting from a Governmental subvention administrated by the French National Research Agency (ANR) within the frame of the 'Future Investments' program (PIA), with the contractual reference 'ANR-11-EQPX-0037'. Chevreul Institute (FR2638), Ministère de l'Enseignement Supérieur et de la Recherche, Région Nord – Pas de Calais and FEDER are acknowledged for supporting and funding partially this work. The authors would like to express their gratitude to Dr. Eric Leroy from ICMPE-CMTR (UMR 7182 CNRS), Martine Trentesaux and Jöelle Thuriot from University of Lille 1 for conducting the STEM-EDS-SDD, XPS and ICP analyses, respectively. Dr Bright Kusema from E2P2L is also acknowledged for performing the recycling tests.

Appendix A. Supplementary materials

Supplementary data associated with this article can be found, in the online version, at <https://doi.org/10.1016/j.jcat.2017.08.015>.

References

- [1] H.A. Wittcoff, B.G. Reuben, J.S. Plotkin, *Industrial Organic Chemicals*, second ed., Wiley, NY, 2004.
- [2] S.A. Lawrence, *Amines: Synthesis, Properties and Applications*, Cambridge University Press, NY, 2004.
- [3] <http://www.ihs.com/products/alkylamines-chemical-economics-handbook.html>.
- [4] K. Eller, E. Henkes, R. Rossbacher, H. Höke, *Amines, Aliphatic*, in: *Ullmann's Encyclopedia of Industrial Chemistry*, Wiley-VCH, Weinheim, 2002.
- [5] K. Visek, *Amines, Fatty*, *Kirk Othmer Encyclopedia of Chemical Technology*, John Wiley & Sons, 2000.
- [6] B.R. Brown, *The Organic Chemistry of Aliphatic Nitrogen Compounds*, Oxford University Press, NY, 1994.
- [7] D.M. Roundhill, *Chem. Rev.* 92 (1992) 1–27.
- [8] T.E. Müller, K.C. Hultzsich, M. Yus, F. Foubelo, M. Tada, *Chem. Rev.* 108 (2008) 3795–3892.
- [9] Y. Huang, W.M.H. Sachtler, *Appl. Catal. A: Gen.* 182 (1999) 365–378.
- [10] P. Roose, M.G. Turcotte, *Amines, Lower Aliphatic*, *Kirk-Othmer Encyclopedia of Chemical Technology*, John Wiley & Sons Inc, 2000.
- [11] K.S. Hayes, *Appl. Catal. A: Gen.* 221 (2001) 187–195.
- [12] M. Pera-Titus, F. Shi, *ChemSusChem.* 7 (2014) 1–4.
- [13] G. Guillena, D.J. Ramón, M. Yus, *Chem. Rev.* 110 (2009) 1611–1641.
- [14] G.E. Dobreiner, R.H. Crabtree, *Chem. Rev.* 110 (2010) 681–703.
- [15] S. Bähn, S. Imm, L. Neubert, M. Zhang, H. Neumann, M. Beller, *ChemCatChem.* 3 (2011) 1853–1864.
- [16] J.L. Klinkenberg, J.F. Hartwig, *Angew. Chem. Int. Ed.* 50 (2011) 86–95.
- [17] C. Gunanathan, D. Milstein, *Science* 341 (2013) 1229712.
- [18] Q. Yang, Q. Wang, Z. Yu, *Chem. Soc. Rev.* 44 (2015) 2305–2329.
- [19] G. Rice, E.J. Koh, *J. Org. Chem.* 77 (1955) 4052–4054.
- [20] A. Mehta, A. Thaker, V. Londhe, S.R. Nandan, *Appl. Catal. A: Gen.* 478 (2014) 241–251.
- [21] G.A. Vedage, L.A. Emig, H-X. Li, J.N. Armor, US 5,917,092, 1998.
- [22] G.A. Vedage, K.S. Hayes, M. Leeaphon, J.N. Armor, US 5,932,769, 1999.
- [23] K.-I. Shimizu, K. Kon, W. Onodera, H. Yamazaki, J.N. Kondo, *ACS Catal.* 3 (2013) 112–117.
- [24] K.-I. Shimizu, K. Kon, W. Onodera, H. Yamazaki, J.N. Kondo, *ACS Catal.* 3 (2013) 998–1005.
- [25] K.-I. Shimizu, *Catal. Sci. Technol.* 5 (2015) 1412–1427.
- [26] A. Baiker, W. Richarz, *Ind. Eng. Chem. Prod. Res. Dev.* 16 (1977) 261–266.
- [27] R.C. Lemon, S. Depot, R.C. Myerly, US 3,022,349, 1982.
- [28] M. Dixit, M. Mishra, P.A. Joshi, D. Shah, *Catal. Commun.* 33 (2013) 80–83.
- [29] F. Santoro, R. Psaro, N. Ravasio, F. Zaccheria, *ChemCatChem.* 4 (2012) 1249–1254.
- [30] A. Baiker, J. Kijenski, *Catal. Rev. Sci. Eng.* 27 (1985) 653–697.
- [31] Y. Li, Q. Li, L. Zhi, M. Zhang, *Catal. Lett.* 141 (2011) 1635–1642.
- [32] J. Sun, X. Jin, F.W. Zhang, W. Hu, J. Liu, R. Li, *Catal. Commun.* 24 (2012) 30–33.
- [33] X. Cui, Y. Dai, Y.Q. Deng, F. Shi, *Chem. Eur. J.* 19 (2013) 3665–3675.
- [34] Q. Li, G. Zhang, S. Peng, J. Surf. Detergents 5 (2002) 229–233.
- [35] J.M. Schwartz, L.D. Schmidt, *J. Catal.* 148 (1994) 22–29.
- [36] J.R. González-Velasco, J.A. Botas, J.A. González-Marcos, M.A. Gutiérrez-Ortiz, *Appl. Catal. B: Environ.* 12 (1997) 61–79.
- [37] S. Wang, G.Q. Lu, *Appl. Catal. B: Environ.* 19 (1998) 267–277.
- [38] H. Xu, K. Shi, Y. Shang, Y. Zhang, G. Xu, Y. Wei, *J. Mol. Catal. A: Chem.* 147 (1999) 41–46.
- [39] K.Y. Koo, H.S. Roh, U.H. Jun, W.L. Yoon, *Catal. Lett.* 130 (2009) 217–221.
- [40] X. Zou, X. Wang, L. Li, K. Shen, X. Lu, W. Ding, *Int. J. Hydrogen Energy* 35 (2010) 12191–12200.
- [41] J. Ashok, S. Kawi, *Int. J. Hydrogen Energy* 38 (2013) 13938–13949.
- [42] I. Luisetto, S. Tuti, C. Battocchio, S. Lo Mastro, A. Sodo, *Appl. Catal. A: Gen.* 500 (2015) 12–22.
- [43] A. Piras, A. Trovarelli, G. Dolcetti, *Appl. Catal. B: Environ.* 28 (2000) L77–L81.
- [44] A. Piras, S. Colussi, A. Trovarelli, V. Sergio, J. Llorca, R. Psaro, L. Sordelli, *J. Phys. Chem. B* 109 (2005) 11110–11118.
- [45] M.C. Sánchez-Sánchez, R.M. Navarro, J.L.G. Fierro, *Int. J. Hydrogen Energy* 32 (2007) 1462–1471.
- [46] Y. Zeng, H. Ma, H. Zhang, W. Ying, D. Fang, *Fuel* 162 (2015) 16–22.
- [47] Y. Le Goff, M. Senes, C. Hamon, US 4209424 A, 1980.
- [48] M.V. Twigg, US 4760190 A, 1988.
- [49] Q. Li, Y. Li, CN 101530800 A, 2009.
- [50] P. Kubanek, W. Mägerlein, J.-P. Melder, T. Herldermann, US 0137029 A1, 2011.
- [51] P. Kubanek, W. Mägerlein, J.-P. Melder, T. Herldermann, US 8318982 B2, 2012.
- [52] C.W. Wigbers, J.-P. Melder, B. Stein, US 0178656 A1, 2013.
- [53] Y.-J. Huang, J.A. Schwarz, J.R. Diehl, J.P. Baltrus, *Appl. Catal.* 36 (1988) 163–175.
- [54] C.-W. Hu, J. Yao, H.-Q. Yang, Y. Chen, A.-M. Tian, *J. Catal.* 166 (1997) 1–7.
- [55] J. Zielinski, *J. Catal.* 76 (1982) 157–163.
- [56] B. Scheffer, P. Molhoek, J.A. Moulijn, *Appl. Catal.* 46 (1989) 11–30.
- [57] J.M. Rynkowski, T. Paryjczak, M. Lenik, *Appl. Catal. A: Gen.* 106 (1993) 73–82.
- [58] B. Vos, E. Poels, A. Bliek, *J. Catal.* 198 (2001) 77–88.
- [59] P.A. Kumar, M.D. Tanwar, N. Russo, R. Pirone, D. Fino, *Catal. Today* 184 (2012) 279–287.
- [60] A. Bensalem, F. Bozon-Verduraz, M. Delamar, G. Bugli, *Appl. Catal. A: Gen.* 121 (1995) 81–93.
- [61] A. Laachir, V. Perrichon, A. Badri, J. Lamotte, E. Catherine, J.C. Lavalley, J. El Fallah, L. Hilaire, F. le Normand, E. Quemere, G.N. Sauvion, O. Touret, *J. Chem. Soc., Faraday Trans.* 87 (1991) 1601–1609.
- [62] K.S.W. Sing, D.H. Everett, R.A.W. Haul, L. Moscou, R. Pierotti, J. Rouquerol, T. Siemieniowska, *Pure Appl. Chem.* 57 (1985) 603–619.
- [63] A. Ponchel, A. D'Huysser, C. Lamonier, L. Jalowiecki-Duhamel, *Phys. Chem. Chem. Phys.* 2 (2000) 303–312.
- [64] M.S. Hegde, G. Madras, K.C. Patil, *Acc. Chem. Res.* 42 (2009) 704–712.
- [65] L. Barrio, A. Kubacka, G. Zhou, M. Estrella, A. Martínez-Arias, J.C. Hanson, M. Fernandez-Garcia, J.A. Rodriguez, *J. Phys. Chem. C* 114 (2010) 12689–12697.
- [66] L.J. Liu, Z.J. Yao, Y. Deng, F. Gao, B. Liu, L. Dong, *ChemCatChem.* 3 (2011) 978–989.

- [67] K.N. Rao, P. Bharali, G. Thrimurthulu, B.M. Reddy, *Catal. Commun.* 11 (2010) 863–866.
- [68] S.K. Mahammadunnisa, P.M.K. Reddy, N. Lingaiah, C. Subrahmanyam, *Catal. Sci. Technol.* 3 (2013) 730–736.
- [69] A. Bensalem, J.C. Muller, F. Bozon-Verduraz, *J. Chem. Soc., Faraday Trans. 88* (1992) 153–154.
- [70] Z.-Y. Pu, J.-Q. Lu, M.-F. Luo, Y.-L. Xie, *J. Phys. Chem. C* 111 (2007) 18695–18702.
- [71] V. Rives, S. Kannan, *J. Mater. Chem.* 10 (2000) 489–495.
- [72] H.C. Yao, Y.F. Yu Yao, *J. Catal.* 86 (1984) 254–265.
- [73] V. Perrichon, A. Laachir, G. Bergeret, R. Frety, L. Tournayan, O. Touret, *J. Chem. Soc., Faraday Trans.* 90 (1994) 773–781.
- [74] K.M. Hardiman, C.G. Cooper, A.A. Adesina, *Ind. Eng. Chem. Res.* 43 (2004) 6006–6013.
- [75] K.M. Hardiman, C.H. Hsu, T.T. Ying, A.A. Adesina, *J. Mol. Catal. A: Chem.* 239 (2005) 41–48.
- [76] A. Zhao, W. Ying, H. Zhang, H. Ma, D. Fang, *Catal. Commun.* 17 (2012) 34–38.
- [77] J. van de Loosdrecht, A.M. van der Kraan, A.J. van Dillen, J.W. Geus, *J. Catal.* 170 (1997) 217–226.
- [78] J. Zhang, H. Xu, X. Jin, Q. Ge, W. Li, *Appl. Catal. A: Gen.* 290 (2005) 87–96.
- [79] K.Y. Koo, H.-S. Roh, Y.T. Seo, D.J. Seo, W.L. Yoon, S.B. Park, *Int. J. Hydrogen Energy* 33 (2008) 2036–2043.
- [80] S. Geller, P.M. Raccah, *Phys. Rev. B* 2 (1970) 1167–1172.
- [81] J.Z. Shyu, W.H. Weber, H.S. Gandhi, *J. Phys. Chem.* 92 (1988) 4964–4970.
- [82] B. Choudhury, A. Choudhury, *Mater. Chem. Phys.* 1131 (2012) 666–671.
- [83] L. Meng, A.-P. Jia, J.-Q. Lu, L.-F. Luo, W.-X. Huang, M.-F. Luo, *J. Phys. Chem. C* 115 (2011) 19789–19796.
- [84] R.K. Pati, I.C. Lee, S. Hou, O. Akhuemonkhan, K.J. Gaskell, Q. Wang, A.I. Frenkel, D. Chu, L.G. Salamanca-Riba, S.H. Ehrman, *ACS Appl. Mater. Inter.* 1 (2009) 2626–2635.
- [85] N. Kaufherr, L. Mendelovici, M. Steinberg, *J. Less Common. Met.* 107 (1985) 281–289.
- [86] F. Le Normand, L. Hilaire, K. Kili, G. Krill, G. Maire, *J. Phys. Chem.* 92 (1988) 2561–2568.
- [87] A. Kotani, T. Jo, J.C. Parlebas, *Adv. Phys.* 37 (1988) 37–85.
- [88] S.A. Krasnikov, A.B. Preobrajenski, T. Chasse, R. Szargan, *Thin Solid Films* 428 (2003) 201–205.
- [89] D. Srinivas, C.V.V. Satyanarayana, H.S. Potdar, P. Ratnasamy, *Appl. Catal. A: Gen.* 246 (2003) 323–334.
- [90] C. Lamonier, A. Ponchel, A. D'Huysser, L. Jalowiecki-Duhamel, *Catal. Today* 50 (1999) 247–259.
- [91] B.M. Reddy, K.N. Rao, G.K. Reddy, A. Khan, S.-E. Park, *J. Phys. Chem. C* 111 (2007) 18751–18758.
- [92] L. Ilieva, G. Pantaleo, R. Nedyalkova, J.W. Sobczak, W. Lisowski, M. Kantcheva, A.M. Venezia, D. Andreeva, *Appl. Catal. B: Environ.* 90 (2009) 286–294.
- [93] J. Xu, B. Xue, Y.-M. Liu, Y.-X. Li, Y. Cao, K.-N. Fan, *Appl. Catal. A: Gen.* 405 (2011) 142–148.
- [94] S. Schimpf, C. Louis, P. Claus, *Appl. Catal. A: Gen.* 318 (2007) 45–53.
- [95] H. Guo, H. Lou, X. Zheng, *Carbon* 45 (2007) 1314–1321.